Realistic Equations of State Informing Neutron Star Post-Merger Gravitational-Wave Frequencies

[arXiv:2602.23646]

S. Magnall, N. Barman, D. Chatterjee, P. Lasky, S. Goode

Nilaksha Barman
Inter-University Centre for Astronomy and Astrophysics (IUCAA)
Pune, India
(Supervisor: Prof. Debarati Chatterjee)

IUCAA

INSTITUTE for NUCLEAR THEORY

INT 26-96W
(June 19th, 2026)

MONASH University

OzGrav
ARC CENTRE OF EXCELLENCE FOR GRAVITATIONAL WAVE DISCOVERY

Hot and Dense environment in Astrophysics

- Neutron Stars (NSs): cold beta equilibrated matter
- Finite Temperature effects:
  - Proto-Neutron Stars (PNSs)
  - Binary Neutron Star (BNS) merger remnants
- Out-of-β-equilibrium ($\mu_p+\mu_e-\mu_n\neq0$)
- Neutrino trapping
- T ~ 0-100 MeV, Y_Q ~ 0.01-0.60, $n_B/n_{sat} \lesssim 6.0$
  - ⇒ Hot NS Configuration

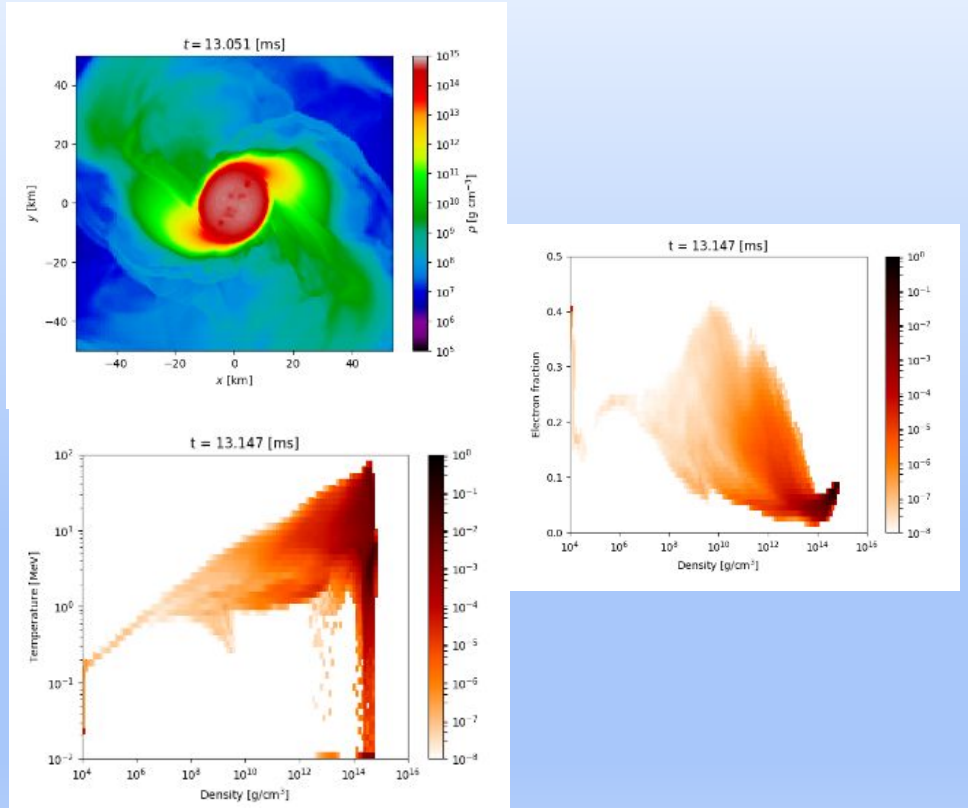

Fig: BNS post-merger
[Credit: Perego et al. (2019)]

General Purpose Equations of State (EOSs)

- Equation of State (EOS) for hot NSs completely specified by - Temperature, density and charge fraction (T, n_B, Y_Q)
- State-of-the-art EOSs available in CompOSE database ⇒ Tabulated EOSs
- These tabulated EOSs use fixed parameterization of nuclear saturation properties
  - might not capture full ranges of uncertainty of nuclear properties based on current multi-messenger data

Nuclear Saturation Properties:

- $\{n_{sat}, E_{sat}, K_{sat}, J_{sym}, L_{sym}, m^*/m\}$+Higher order terms→Cold EoS
- n_{sat} = nuclear saturation density
- E_{sat} = Binding energy at saturation for SNM
- K_{sat} = Curvature of Binding energy at saturation for SNM
- J_{sym} = Symmetry energy at saturation
- L_{sym} = Slope of Symmetry energy at saturation
- m^*/m = effective nucleon mass (Dirac)

	n_{sat} (fm^{-3})	E_{sat} (MeV)	K_{sat} (MeV)	J_{sym} (MeV)	L_{sym} (MeV)	m^*/m
Fixed	0.15	−16.0	240	32	60	0.65
Varied	0.14–0.17	-16 ± 0.2	200–300	28–34	40–70	0.55–0.75

Table: Uncertainty ranges or priors of nuclear parameters (Ghosh+ 2022)

Constraints on EOS

Constraints at different densities

- Chiral Effective Field Theory (χEFT):
  Robust microscopic calculations at low density (0.07-0.20 fm^{-3}) in Pure Neutron Matter (PNM)
- Astrophysical Observations (Astro):
  High density constraints from Maximum NS mass (PSR J0740+6620), Radius and Tidal Deformability of GW170817
- Heavy Ion Collision (HIC):
  Intermediate density (1-3 n_{sat}) constraints from KaoS, FOPI, ASY-EOS experiments at GSI, Germany

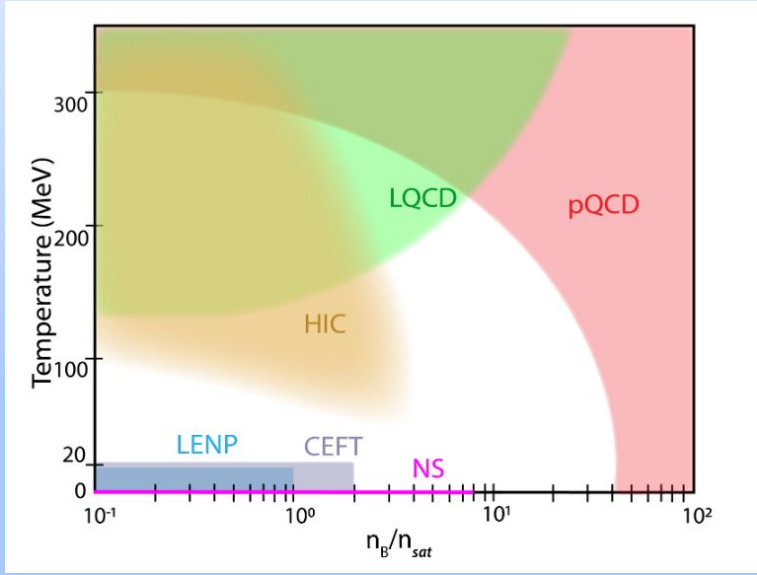

Fig: QCD phase diagram
[MUSES Collab.]

Equation of State (EOS) Model

- Non-linear Relativistic Mean Field (NL-RMF) model
  - Nucleon-nucleon interaction through meson exchange
  - Applied to constrain properties of cold NSs (Ghosh+ 2022 , Maiti+ 2026)
  - Finite T extension: Barman+ 2025, Barman & Chatterjee (2025)

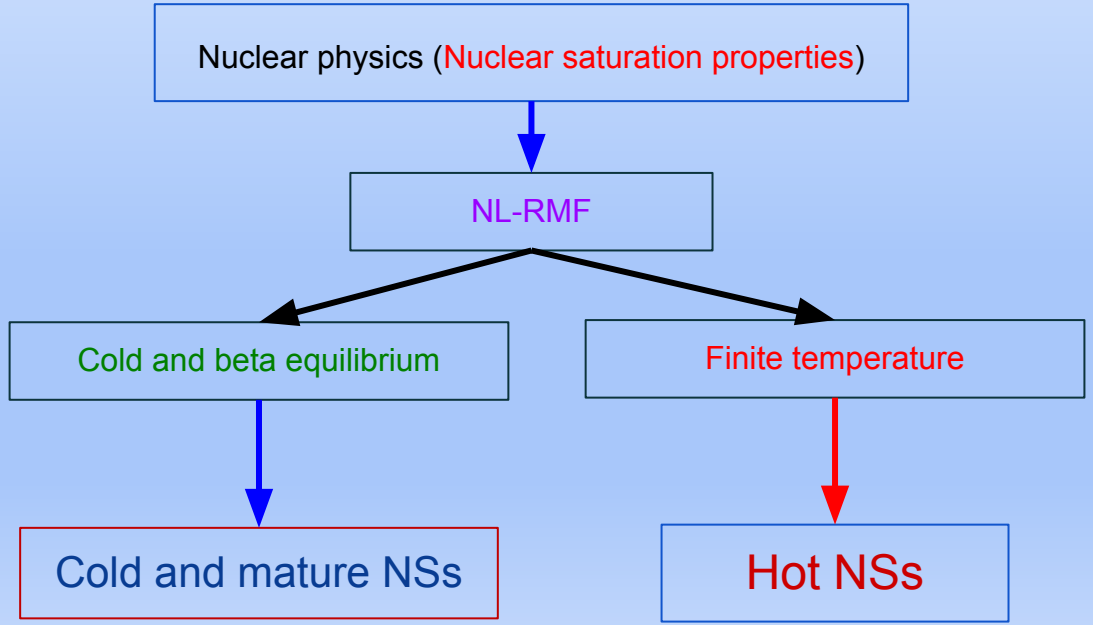

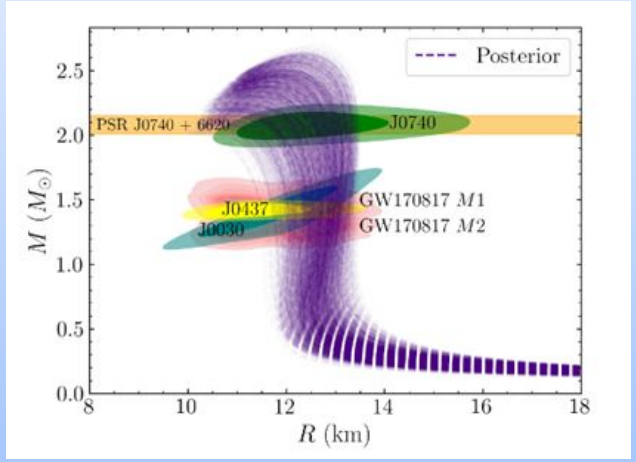

Fig: Mass-Radius posteriors for cold NSs on imposing Astro + χEFT constraints [Maiti+ 2026]

Macroscopic/microscopic properties of hot NSs

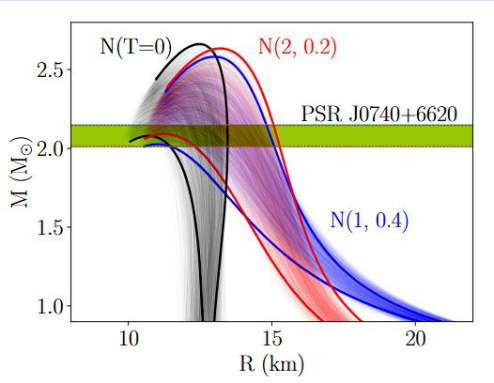

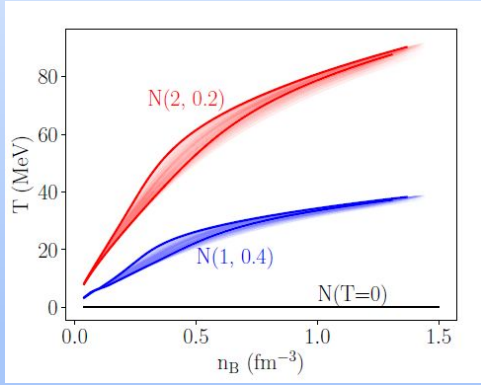

Fig: Mass-Radius and T vs n_B posteriors for T = 0; S/A = 2,Y_Q= 0.2 and S/A = 1,Y_Q= 0.4 for nucleonic (N) matter from χEFT + Astro constraints

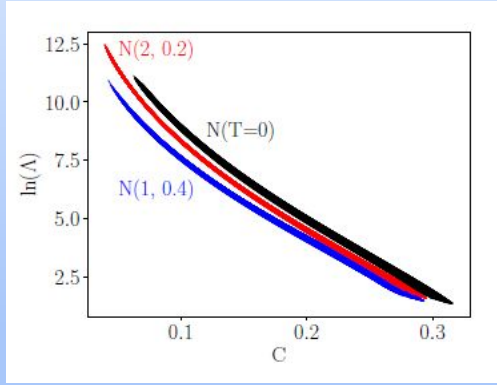

Fig: C-Love relations (χEFT + Astro)

N. Barman, B.K. Pradhan, D. Chatterjee; (2025)

Application to BNS post-merger GW signals?

BNS post-merger scenario

- Inspiral -> merger -> post-merger -> Prompt collapse/Long-lived NS

- Long-lived NSs:
  - HMNS (metastable)
  - SMNS (metastable)
  - Stable NSs

- Hot (T≲100 MeV) and rapidly rotating

- Timescale ~ 0 - 100 ms

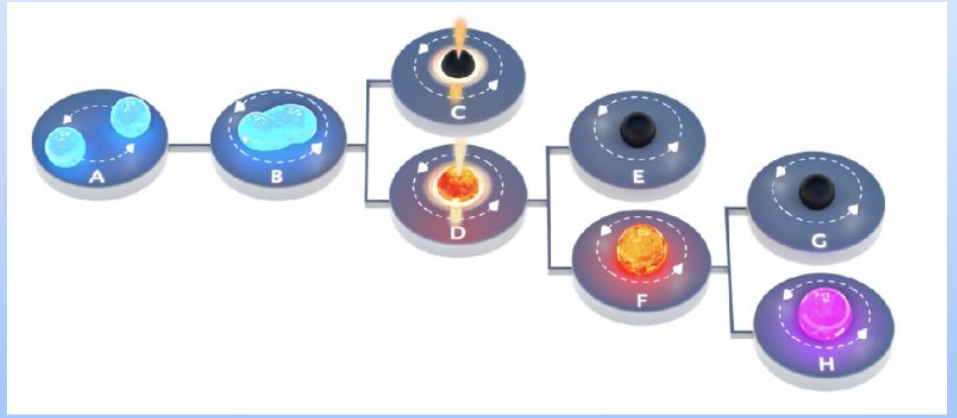

Sarin & Lasky, 2021

GWs from BNS post-merger scenarios

- Frequency peaks
- Peak GW frequency emission through quadrupolar f-mode from the hot and rapidly rotating remnant (Pointed out by Stergioulas+ 2011, Bernuzzi+ 2015)
- $f_{peak} = f_2$ -> Nuclear EOS
- High frequency region

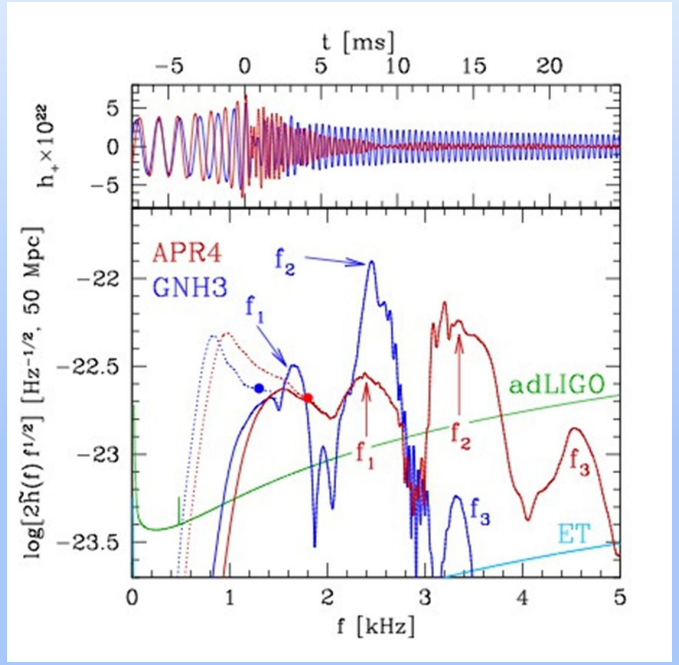

Fig: BNS post-merger signal (Takami+ 2014)

Post-merger spectra

- Numerical relativistic hydrodynamic simulations:
  - Computationally expensive
  - Limited in number
  - EOS uncertainty

- We assume
  - Approximate thermal profile seen in simulations (Most+ 2023)
    - Cold: N(S/A = 0)
    - Warm: N(S/A = 1)
    - Hot: N(S/A = 2)

  - Rotation close to Kepler frequency

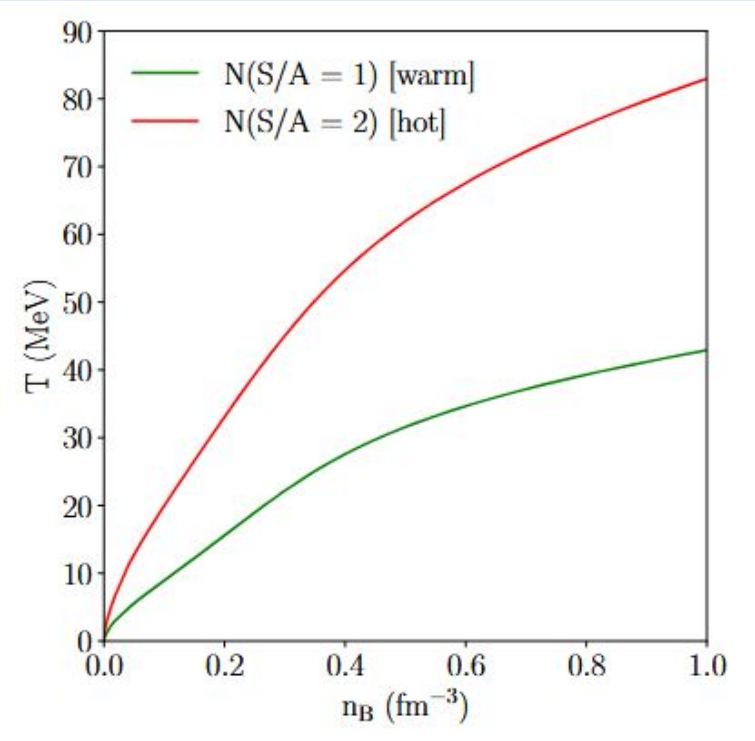

Determination of f_{peak}

- We assume that the l = |m| = 2, f-mode is the peak frequency
  - Calculated using Doneva+ 2013 fits
  - Keplerian rotation

- Remnant mass ~ 2.2 - 3 solar mass (drawn uniformly)

- EOS posteriors ~ 3300 EOSs each [χEFT+ Astro]

- f_{peak} as a function of remnant mass

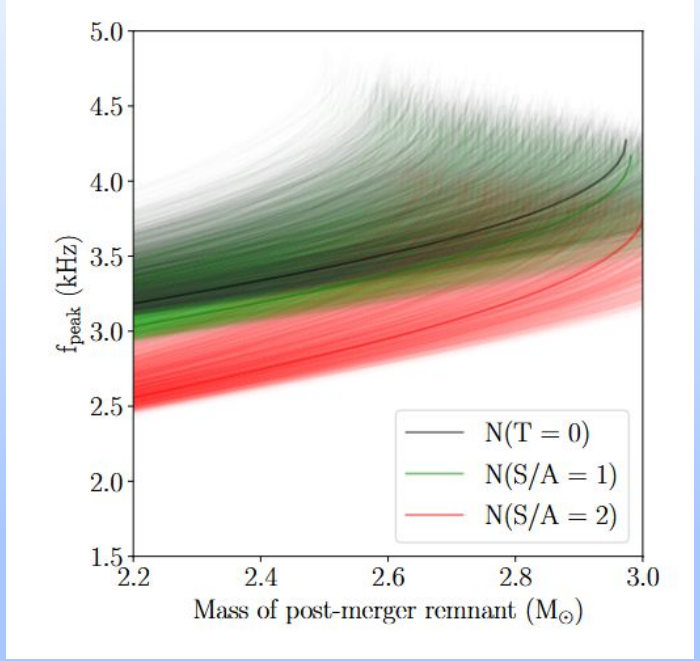

Finite T effect: Reduction of f_{peak} by ~ 200-600 Hz

f_{peak} distribution

- 90% Confidence Intervals (CIs):
  - f_{peak} (cold): 3627^{+581}_{-389} Hz
  - f_{peak} (warm): 3476^{+591}_{-397} Hz
  - f_{peak} (hot): 3039^{+633}_{-424} Hz

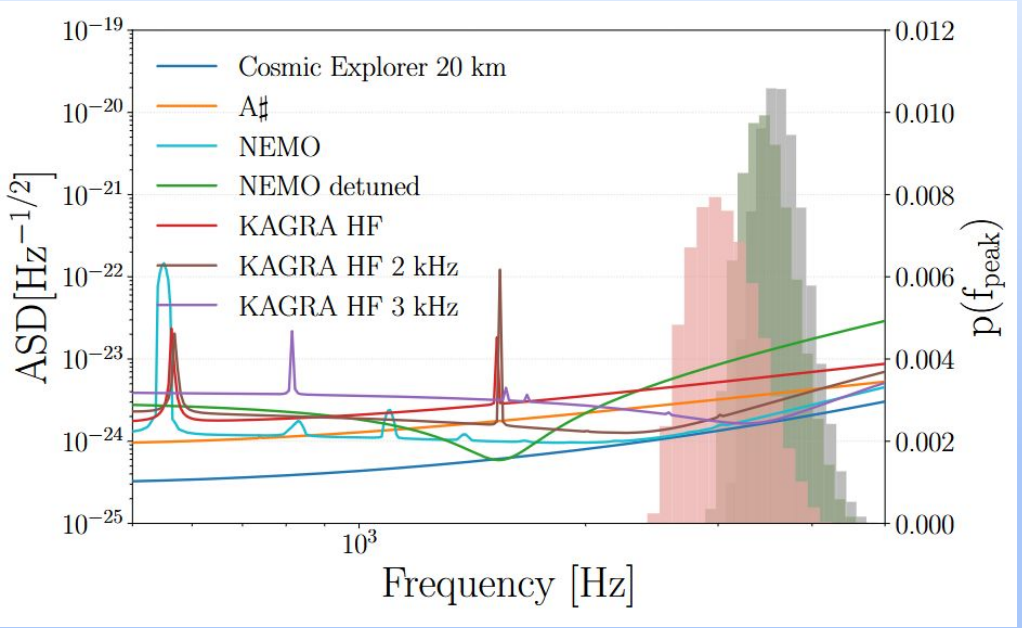

Implication(s) on High frequency detuned detector configuration(s)

High frequency (HF) detectors

- We need highly sensitive detectors at high frequency!

- Dedicated HF detectors have been proposed: CE,ET, NEMO, KAGRA HF etc.

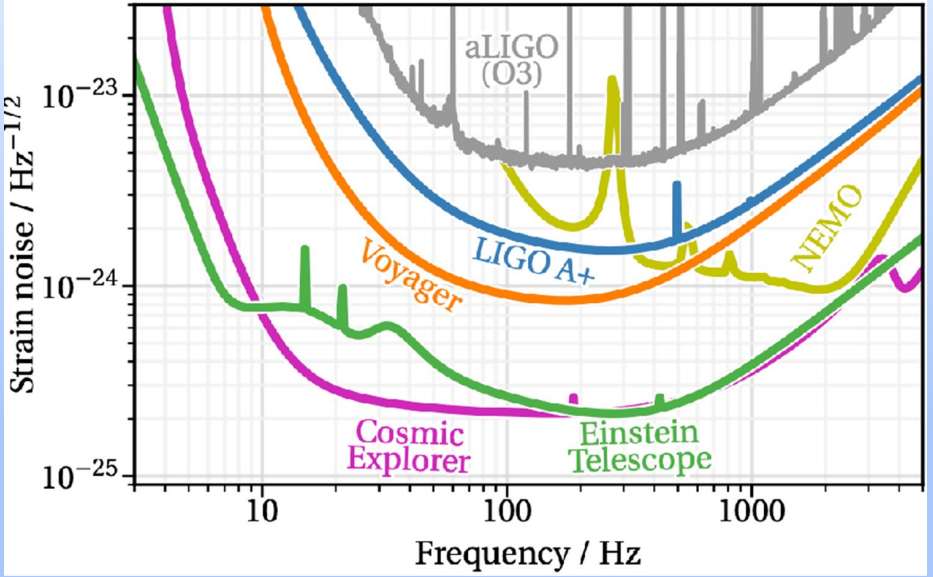

Detuning of detectors

- Detuning:
  - increasing sensitivity at certain frequencies, but compromising inspiral sensitivity
  - Reasonable estimates for where to tune is needed for post-merger scenarios
  - Proposed for NEMO and KAGRA HF

Broadband vs detuned/narrowband configuration?

Detuned post-merger optimized (PMO) detector configuration: KAGRA HF

- Synthetic Post-merger signal:
  - Damped sinusoid in time domain with frequency = f_{peak}
  - Damping timescale ~ 0.025s
- ~10^5 binary injection sets for each cold, warm and hot EOSs
- PMO: KAGRA HF 2 kHz and 3 kHz

$$\rho_{\mathrm{norm}} = \frac{\rho_{\mathrm{PMO}}}{\rho_{\mathrm{BB}}}, \quad (8)$$

where ρ_{PMO} is the signal-to-noise ratio of the injection in the post-merger optimised detector, and ρ_{BB} is the signal-to-noise ratio of the injection in the broadband configuration.

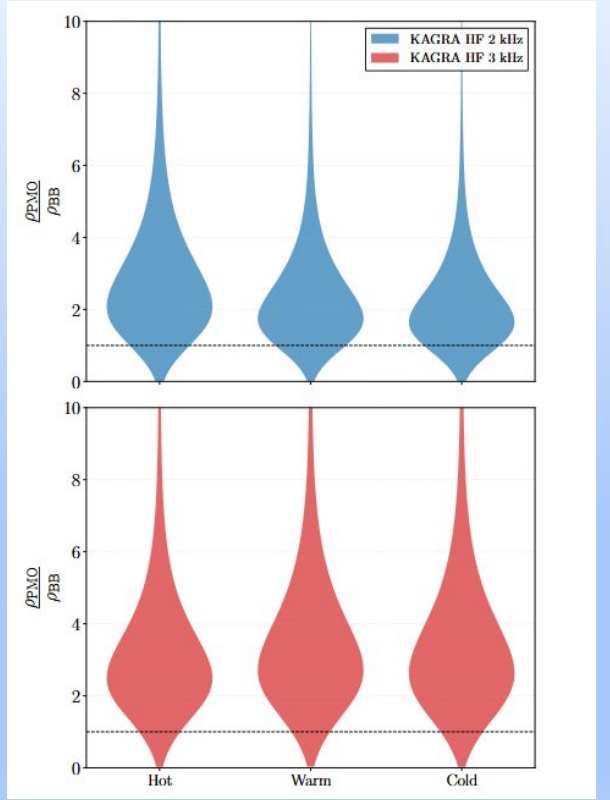

3 kHz detuned detector gives a median ~ 3 times improvement in optimal SNR across all temperatures

Summary

- We estimated peak GW frequency from BNS post-merger signal taking into account finite T behaviour: ~ 2.5 - 4 kHz

- Median of f_{peak} ~ 3 kHz with S/A = 2
- With finite T, f_{peak} is reduced by ~ 200-600 Hz compared to zero temperature estimation

- 3 kHz detuned KAGRA HF detector gives ~ 3 times improvement in optimal SNR across all temperatures

- For 2 kHz configuration, it is ~ 2 times

Thanks

Extra Slides

Equation of State Modelling

- Non-linear Relativistic Mean Field (NL-RMF) model fitted to reproduce nuclear saturation properties (Chen and Piekarewicz 2014, Hornick+2018)

$$\mathcal{L} = \sum_B \bar{\psi}_B(i\gamma_\mu\partial^\mu - m_B + g_{\sigma B}\sigma - g_{\omega B}\gamma^\mu\omega_\mu - g_{\phi B}\gamma^\mu\phi_\mu - g_{\rho B}\gamma^\mu\rho_\mu^a\tau^a)\psi_B + \frac{1}{2}\partial^\mu\sigma\partial_\mu\sigma - \frac{1}{2}m_\sigma^2\sigma^2 - \frac{1}{4}\omega_{\mu\nu}\omega^{\mu\nu} + \frac{1}{2}m_\omega^2\omega^2 - \frac{1}{2}\vec{\rho}_{\mu\nu}\vec{\rho}^{\mu\nu} + \frac{1}{2}m_\rho^2\vec{\rho}^2 - \frac{1}{4}\phi_{\mu\nu}\phi^{\mu\nu} + \frac{1}{2}m_\phi^2\phi^2 + U_\sigma + \Lambda_\omega(g_{\rho N}^2\vec{\rho}_\mu\cdot\vec{\rho}^\mu)(g_{\omega N}^2\omega_\mu\omega^\mu) + \sum_L \bar{\psi}_L(i\gamma_\mu\partial^\mu - m_L)\psi_L + \sum_{i=B,L}\bar{\psi}_i(-q_i\gamma_\mu A^\mu)\psi_i - \frac{1}{4}F_{\mu\nu}F^{\mu\nu}$$

	n_{sat} (fm^{-3})	E_{sat} (MeV)	K_{sat} (MeV)	J_{sym} (MeV)	L_{sym} (MeV)	m^*/m
Fixed	0.15	−16.0	240	32	60	0.65
Varied	0.14–0.17	-16 ± 0.2	200–300	28–34	40–70	0.55–0.75

Table: Uncertainty ranges or priors of nuclear parameters (Ghosh+ 2022)

- $U_\sigma = \frac{1}{3}\, b m_N \sigma^3 + \frac{1}{4}\, c\sigma^4$
- Isoscalar channel: $\{g_\sigma, g_\omega, b, c\} \rightarrow \{n_{sat}, E_{sat}, K_{sat}, m^*/m\}$
- Isovector channel: $\{g_\rho, \Lambda_\omega\} \rightarrow \{J_{sym}, L_{sym}\}$

$$U_i^N = -g_{\sigma i}\bar{\sigma}_0 + g_{\omega i}\bar{\omega}_0$$

Equation of State Modelling (Continued)

Entropy density:

$$
\begin{aligned}
s = & -\sum_{i\in B} \frac{2J_i+1}{2\pi^2} \int dk k^2 \left[f_{FD}\left(\frac{E_i(k)-\mu_i^*}{T}\right) \right. \\
& \ln f_{FD}\left(\frac{E_i(k)-\mu_i^*}{T}\right) + \bar{f}_{FD}\left(\frac{E_i(k)-\mu_i^*}{T}\right) \\
& \left. \ln \bar{f}_{FD}\left(\frac{E_i(k)-\mu_i^*}{T}\right) \right] \\
& + anti-baryon\ contribution\ (\mu_i^* \to -\mu_i^*) \\
& + s_{e^-} + s_{e^+} \\
& + s_\gamma \ ,
\end{aligned}
$$

EoS:

$$
\begin{aligned}
\epsilon = & < T^{00} > \\
& = \frac{1}{2} m_\sigma^2 \bar{\sigma}^2 + \frac{1}{2} m_\omega^2 \bar{\omega}_0^2 + \frac{1}{2} m_\rho^2 \bar{\rho}_{03}^2 + U_\sigma \\
& + 3\Lambda_\omega (g_{\rho N} g_{\omega N} \bar{\rho}_{03} . \bar{\omega}_0)^2 \\
& + \sum_i \frac{2J_i+1}{2\pi^2} \int dk k^2 E_i(k) \left[f_{FD}\left(\frac{E_i(k)-\mu_i^*}{T}\right) \right. \\
& \left. + f_{FD}\left(\frac{E_i(k)+\mu_i^*}{T}\right) \right] \\
& + \epsilon_{e^-} + \epsilon_{e^+} \\
& + \epsilon_\gamma \ , \\
p = & \sum_{i=B,e} \mu_i n_i + Ts - \epsilon \ .
\end{aligned}
$$

Doneva fit

$$\frac{\sigma_{\rm corot}}{\sigma_0} = 1 - 0.235\left(\frac{\Omega}{\Omega_k}\right) - 0.358\left(\frac{\Omega}{\Omega_k}\right)^2, \quad (1)$$

where σ_0 is the oscillation frequency of the f-mode for the non-rotating case, Ω is the hypermassive neutron star rotation frequency and Ω_k is the break up frequency of the neutron star (Kepler frequency). We approximate this Kepler frequency using the relation derived in Doneva et al. (2013)

$$\frac{1}{2\pi}\Omega_k\,[\mathrm{kHz}] = 1.716\left(\frac{M_0}{1.4\ M_\odot}\right)^{1/2}\left(\frac{R_0}{10\ \mathrm{km}}\right)^{-3/2} - 0.189, \quad (2)$$

where M_0 and R_0 are the mass and radius of the non-rotating model, respectively. The mass scaling with rotation frequency of the neutron star is given by,

$$\frac{M}{M_0} = 0.991 + 9.36\times10^{-3}\exp\left(3.28\frac{\Omega}{\Omega_K}\right), \quad (3)$$

where M is the mass of the rotating neutron star . The frequency for the non-rotating $l = |m| = 2$ is given by

$$\frac{1}{2\pi}\sigma_0\,[\mathrm{kHz}] = 1.562{+}1.151\left(\frac{M_0}{1.4\,M_\odot}\right)^{1/2}\left(\frac{R_0}{10\,\mathrm{km}}\right)^{-3/2}. \quad (4)$$

Assuming a remnant rotating at the Kepler frequency and substituting Ω_k and σ_0 into Equation 1, we then convert from the co-rotating frame to the inertial frame

$$\sigma_{\rm inert} = \sigma_{corot} - m\Omega. \quad (5)$$

Motivation: Unstable oscillation modes and Gravitational wave (GW) emission

- Fundamental mode: f-mode (1-3 kHz)
- The frequencies strongly depend on the particular cold EOS i.e. nuclear parameters

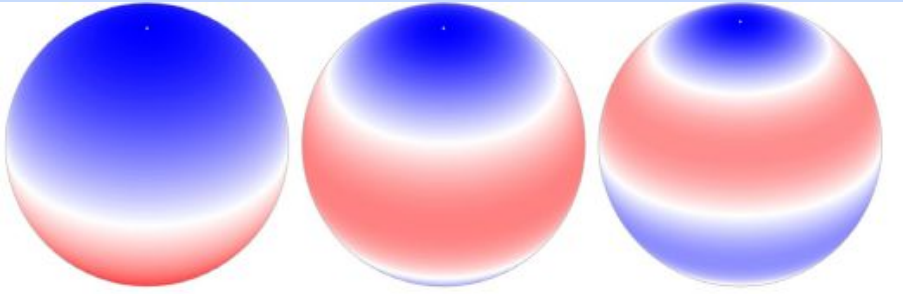

Fig: *l* = 1, 2, 3 modes [credit: C. Aerts]

Band corresponds to uncertainty in nuclear EOS

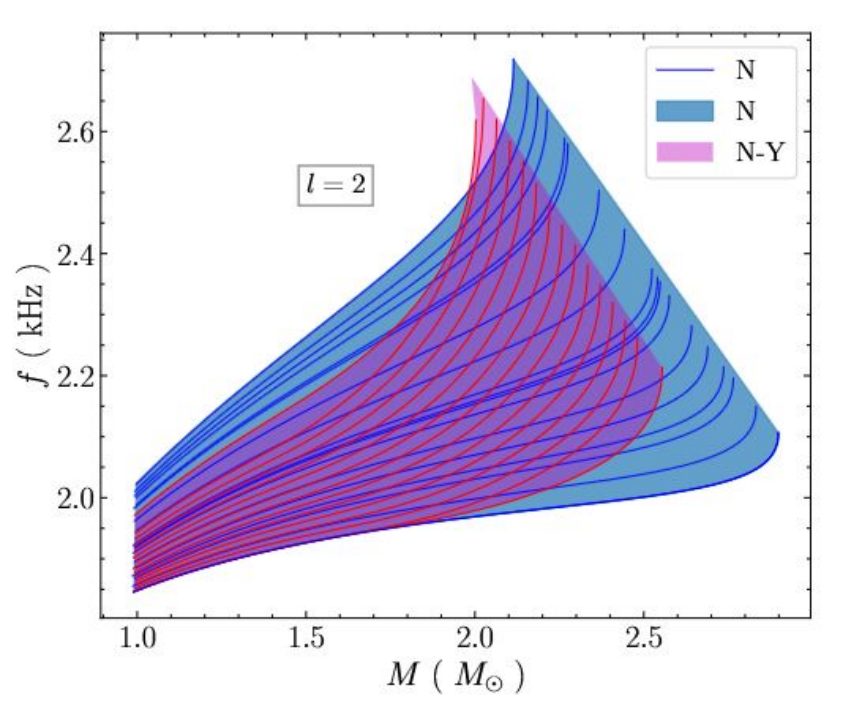

f-mode frequency vs mass for cold NSs (Pradhan+ 2021)

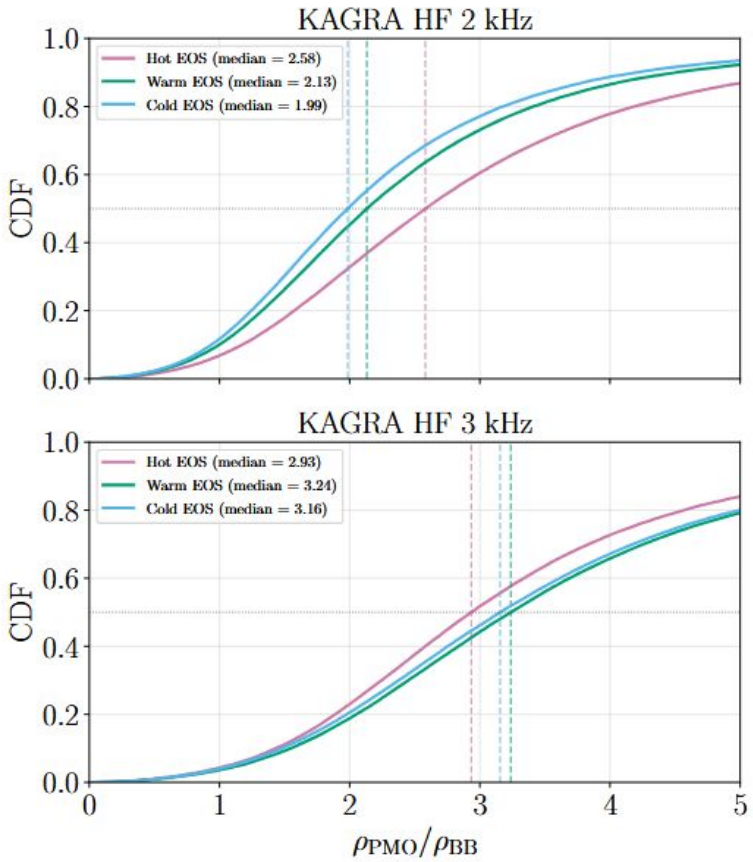

Figure 5. Cumulative distribution function plots of expected signal-to-noise ratios of post-merger remnants for our EoSs. The signal-to-noise ratios for the post-merger optimised detectors are normalised against the standard or 'broadband' configuration of the detector. The top panel corresponds to a 2 kHz configuration of the KAGRA HF detector whereas the bottom panel corresponds to a 3 kHz configuration of the KAGRA HF detector. Each panel contains three CDFs representing the hot ($S/A = 2$),warm ($S/A = 1$), and cold ($S/A = 0$) equations of state. The coloured dashed lines represent the median normalised signal-to-noise ratio of each equation of state set.

CE 20 vs NEMO vs KAGRA HF